Heliyon 9 (2023) e20994

Contents lists available at ScienceDirect

Heliyon

journal homepage: www.cell.com/heliyon

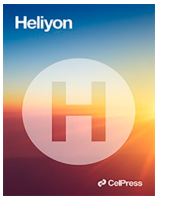

Performance analysis of digitally controlled nonlinear systems considering time delay issues

Cağfer Yanarateş [a], Serkan Okur [b], Aytaç Altan [b,*]

[a] Department of Electrical and Energy, Kelkit Aydın Doğan Vocational School, Gümüşhane University, 29600, Gümüşhane, Turkey
[b] Department of Electrical Electronics Engineering, Zonguldak Bülent Ecevit University, 67100, Zonguldak, Turkey

ARTICLE INFO

Keywords:
Nonlinear systems
Switch mode power supply
Discretization techniques
System delays
Effective sample time selection

ABSTRACT

In this paper, a comprehensive investigation into discretization, effective sample time selection considering delays in the system, and time and frequency domain analysis of a DC-DC buck converter, which plays a vital role in photovoltaic (PV) systems, is conducted to enhance the understanding of their dynamic behavior, optimize control algorithms, improve system efficiency, and ensure reliable power conversion in photovoltaic applications. To effectively address the non-linear behavior and enhance digital control of a buck converter by selecting the best sample time, several approaches can be employed. These include accurate modeling and identification of non-linear elements, development of advanced control algorithms that account for non-linearities, implementation of adaptive control techniques, and utilization of feedback mechanisms to compensate for deviations from linearity. By considering and mitigating the non-linear behavior, digital control systems can achieve improved accuracy, stability, and transient behavior in regulating the buck converter's output waveforms (voltage or current). The results of the study demonstrated that the trapezoidal integration method which is also known as bilinear approximation, or Tustin's approach outperformed other commonly used discretization methods, such as first-order hold (FOH), zero-order hold (ZOH), impulse response matching (impulse invariant), and matched pole-zero (MPZ) technique, in dual-domain (both time and frequency) analysis. The key finding highlighting the superiority of the bilinear approximation was its ability to achieve the closest match in the frequency domain bridging the continuous-time and discrete systems. This finding emphasizes the significance of the bilinear approach in preserving the frequency characteristics of the original continuous-time system during discretization. By employing this method, the discrete system closely approximated the behavior of its continuous-time counterpart, ensuring accurate frequency-domain representation.

1. Introduction

In the past few decades, there has been a significant emphasis on obtaining electrical energy from renewable sources due to the surge in energy requirements and the growing interest in sustainable energy production. This shift is driven by the need to reduce carbon emissions and mitigate the environmental impact of conventional power sources. Among the various sustainable energy options, solar power has emerged as a highly promising and environmentally friendly source of clean energy with tremendous potential.

* Corresponding author.
E-mail addresses: cagferyanarates@gumushane.edu.tr (C. Yanarateş), s.okur@fbe.karaelmas.edu.tr (S. Okur), aytacaltan@beun.edu.tr (A. Altan).

https://doi.org/10.1016/j.heliyon.2023.e20994
Received 16 July 2023; Received in revised form 29 August 2023; Accepted 12 October 2023
Available online 13 October 2023

To fully harness the benefits of solar energy, extensive research efforts have been dedicated to two key areas: maximum power point tracking (MPPT) applications and the integration of solar energy into smart grids. These research endeavors primarily revolve around evaluating the performance of PV systems, which play a critical role in effectively capturing and utilizing solar energy [1–3].

Switch mode power supplies (SMPS) play a crucial role in PV systems, contributing to their overall performance, efficiency, and reliability. SMPS devices, such as DC-DC converters and DC-AC inverters, efficiently convert the DC power produced by PV modules into the needed required AC power, optimizing energy conversion, and minimizing power losses. SMPS-based peak power tracking controllers dynamically adjust the voltage and current to extract the maximum available power from the PV modules, enhancing energy yield and system efficiency [3–6].

SMPS devices also provide voltage regulation and stabilization, ensuring a consistent voltage level for downstream components and loads, thereby maintaining reliable and stable power delivery. They incorporate various protection features, such as overvoltage, overcurrent, and short-circuit protection, safeguarding the PV system and its components. This enhances system reliability and safety. Additionally, SMPS devices facilitate the integration of PV systems with the grid and energy storage solutions. They enable efficient power transfer between the PV system, grid, and battery systems, optimizing energy flow and enabling functionalities like grid feed-in, load balancing, and energy management [7].

SMPS are devices that employ high frequency switching to efficiently and reliably convert electrical energy. Due to the nonlinearity and inherent delays within these systems, their analysis becomes complex and necessitates careful consideration [8]. In particular, delays can significantly impact the accuracy of control algorithms and result in undesirable outcomes. Consequently, it is imperative to employ suitable approaches and methods for the analysis and control of nonlinear systems [8]. In this context, it becomes crucial to investigate the dual-domain response of the system, assess both distorting and non-distorting delays, and evaluate discretization techniques that influence controller performance.

The time response of a system provides valuable information about its behavior over time in response to input changes, shedding light on both transient and steady-state dynamics. It offers insights into how the system reacts, settles, and stabilizes following perturbations. Conversely, the frequency response of a system describes its ability to process signals at various frequencies, revealing crucial characteristics such as gain, phase shift, and resonance properties. These response characteristics are fundamental in assessing the performance and stability of nonlinear systems, aiding in the analysis, design, and optimization of control strategies and system parameters [9].

Delays are frequently encountered in practical applications due to factors like signal propagation, processing time, and system constraints. These delays can have a substantial impact on the performance of nonlinear systems, leading to challenges such as instability, oscillations, or reduced accuracy. Consequently, it is of utmost importance to thoroughly understand and analyze the effects of these delays on system performance. This understanding is crucial for designing robust control strategies that can effectively mitigate the adverse effects of delays and ensure the desired behavior of the system. By comprehensively examining the effects of delays, engineers can develop control systems that are resilient, accurate, and capable of achieving the desired system behavior in practical applications [10].

In the analysis of nonlinear systems, an additional crucial aspect to consider is discretization, which involves converting continuous-time systems into discrete-time representations [11]. Discretization becomes particularly significant when implementing systems on digital platforms, where continuous-time signals need to be sampled and computations must be performed at specific time intervals [12]. The selection of appropriate discretization techniques holds substantial implications for the accuracy, stability, and overall performance of nonlinear systems [13]. Various studies have demonstrated the impact of discretization methods on system behavior, emphasizing the need for careful evaluation and selection [14]. Moreover, the connection between discretization, control strategies, and real-world applications has been extensively discussed, further highlighting the critical role of this process in system design [15]. Therefore, a thorough understanding of discretization techniques and their effects is essential when analysing and designing nonlinear systems.

Discretization serves as a bridge between the continuous and discrete domains, enabling the representation and processing of system dynamics in a time-discrete manner. By discretizing the system, continuous-time signals are transformed into a sequence of discrete values, which facilitates their representation and manipulation using digital algorithms. This becomes essential when implementing control systems, simulations, or numerical analyses on digital platforms [16]. The choice of discretization techniques can significantly impact the behavior and performance of nonlinear systems. Each technique introduces a certain level of approximation and truncation error due to the finite time step used in the discretization process. The accuracy of the discretized representation depends on factors such as the chosen discretization technique, the time step size, and the characteristics of the original continuous-time system [17]. Furthermore, the stability of the discrete-time system must be considered. Stability concerns arise due to the discretization process potentially introducing additional dynamics and amplifying certain frequency components, leading to instability issues. Therefore, it is essential to choose discretization techniques that preserve stability or employ additional stabilization methods to ensure the stable operation of the discrete-time system [18].

The objective of this study is to conduct a comprehensive comparative assessment analysis of nonlinear systems, specifically focusing on their time and frequency response, the influence of system delays, and the effectiveness of various discretization techniques in the context of a commonly employed DC-DC buck converter in PV system applications. By means of thorough investigations, precise mathematical modeling, and simulation studies, the objective is to evaluate the performance of diverse nonlinear systems and provide insights into the ramifications of these factors on system behavior.

The primary contributions of this study can be outlined as follows:

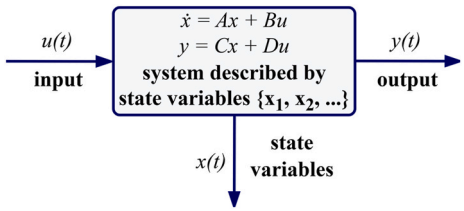

Fig. 1. The general state-space representation.

Table 1
The diagram depicting the procedural steps of the state-space averaging method.

1. Description of notations	2. ON and OFF states	3. Basic averaged model
$d \equiv$ *duty ratio* $d' \equiv 1 - d$ $T_s \equiv$ *switching period*	Interval dT_s $\dot{x} = A_1x + B_1v_{in}$ Interval $d'T_s$ $\dot{x} = A_2x + B_2v_{in}$	$\dot{x} = Ax + Bv_{in}$ $A = dA_1 + d'A_2$ $B = dB_1 + d'B_2$
4. Perturbation	**5. Steady-state DC model**	**6. AC small signal model**
$d = D + \hat{d}$ $x = X + \hat{x}$ $y = Y + \hat{y}$ $v_{in} = V_{in} + \hat{v}_{in}$	$AX + BV_{in} = 0$ $X = -A^{-1}BV_{in}$	$\dot{\hat{x}} = A\hat{x} + B\hat{v}_{in} +$ $[(A_1 - A_2)X + (B_1 - B_2)V_{in}]\hat{d}$

- Comprehensive comparative assessment analysis: This research undertakes an extensive comparative assessment analysis of nonlinear systems, with a specific focus on their time and frequency responses, the impact of system delays, and the efficacy of various discretization techniques. The goal is to provide a thorough understanding of how nonlinear systems behave under different conditions and how these behaviors compare.
- Application to PV system buck converter: The study's context is particularly relevant to practical applications as it examines the behavior of nonlinear systems in the context of a widely used DC-DC buck converter within photovoltaic (PV) system applications. This practical relevance bridges theoretical analysis with real-world applications.
- Exploration of time and frequency responses: By scrutinizing the time and frequency responses of nonlinear systems, this research delves into the temporal and spectral characteristics of such systems. This investigation provides insights into how these systems behave over time and in various frequency ranges.
- Analysis of system delay effects: The research investigates the influence of system delays on nonlinear system performance. Understanding how delays affect these systems can have significant implications for their real-world implementation and control.
- Effectiveness of discretization techniques: The study evaluates the effectiveness of different discretization techniques when applied to nonlinear systems. This assessment is crucial for determining suitable methods for transforming continuous-time systems into discrete-time representations.
- Utilization of mathematical modeling and simulation: Through precise mathematical modeling and simulation studies, the research seeks to accurately represent the behavior of nonlinear systems and assess their performance. These techniques offer a comprehensive way to analyze system dynamics.
- Insights into system behavior ramifications: The overall objective of the study is to provide insights into how various factors influence the behavior of nonlinear systems. By doing so, the research aims to contribute to the broader understanding of nonlinear dynamics and its implications for system design and operation.

By addressing these key aspects, the paper aims to enhance our understanding of nonlinear system behavior and its impact on practical applications, ultimately contributing to improved system analysis, design, and implementation.

The remainder of this paper is organized as follows. Section 2 describes the derivation of the transfer function of the small-signal duty cycle to inductor current in PWM buck converter. Delays in digital control systems are presented in Section 3. The implementation of various discretization techniques for the proposed buck converter is given in Section 4. Section 5 focuses on PI controller design and performance analysis of the controller. The results of the study and some concrete discussions are mentioned in Section 6. Conclusions and future work are highlighted in Section 7.

2. Transfer function of small-signal duty cycle to inductor current in PWM buck converter

System analysis involves creating an accurate mathematical model that captures the real-world behavior of a plant. This process, known as system modeling, enables us to describe the system mathematically. A well-developed model allows us to predict and observe the plant's response in both the time and frequency domains. The transfer function of the plant establishes the relationship between its input and output, providing valuable insights into its dynamics. A precisely derived transfer function is essential for designing effective controllers. Control systems are designed and implemented to improve crucial dynamic characteristics of the plant, including stability,

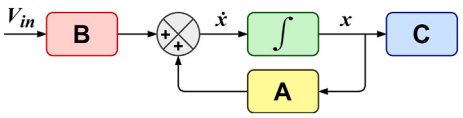

Fig. 2. The vector diagram representing the state-space of a linear system.

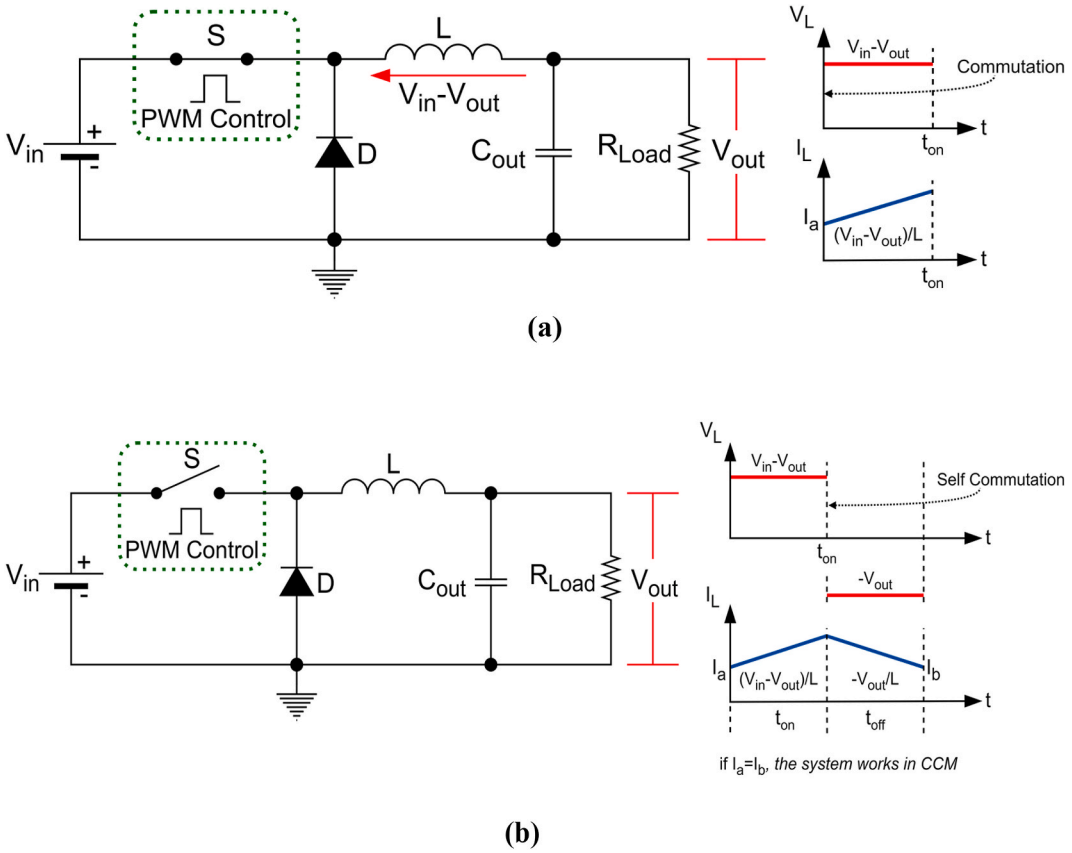

Fig. 3. Switching configurations and waveforms of the inductor current and voltage in CCM **(a)** on-state, **(b)** off-state.

response speed, steady-state error, and oscillations, encompassing both transient and steady-state responses [19].

2.1. State-space average modelling of switch mode power supplies

The transfer function model of the desired buck converter is obtained through the application of the dynamic (AC small signal) state-space methodology [20–22]. In this procedure, the Laplace transform (with an initial condition of zero) is applied to both the state and output equations within the state-space representation of the buck converter [23,24]. Fig. 1 presents the most general and comprehensive state-space depiction of a system with p inputs, q outputs, and n state variables.

Here $A(.)$, $B(.)$, $C(.)$, and $D(.)$ are state matrix with $dim[A(.)] = n \times n$, input matrix with $dim[B(.)] = n \times p$, output matrix with $dim[C(.)] = q \times n$ and feedforward matrix with $dim[D(.)] = q \times p$, respectively. $x(.)$, $y(.)$, and $u(.)$ are state vector with $x(t) \in \mathbb{R}^n$, output vector with $y(t) \in \mathbb{R}^q$, control vector with $u(t) \in \mathbb{R}^P$, respectively. The process depicting the procedural steps of the state-space averaging method is presented Table 1.

Fig. 2 illustrates the vector block diagram representing the state-space dynamics of a linear-time-invariant system, while Equation (1) presents the average state-space equation for the system.

$$\dot{x} = Ax + Bv_{in} \tag{1}$$

$$y = Cx$$

Equation (1) characterizes the averaged performance of the SMPS, aiming to eliminate the inherent ripples present in the capacitor voltage and inductor current, which arise from the properties of the state variables. It is noteworthy that the matrices A and B can vary

Table 2
The derived values for the parameters and components of the proposed buck converter.

Variables and Constituents	Values
Duty cycle in steady state	0.6042
Minimum load inductor current in average (A)	7.3483
Minimum load inductor current ripple in average (A)	1.4697
Inductance (mH)	0.781
Output voltage fluctuation (V)	1.16
Capacitance (μF)	15.837

with the duty ratio (d), implying that the averaged equation may exhibit non-linear characteristics in relation to the duty ratio.

2.2. Calculations of the proposed buck converter's power stage

The buck converter is a switching topology that takes a DC input voltage, V_{in}, and converts it to a lower DC output voltage, V_{out}. In an asynchronous buck converter, a diode serves as the lower switch, automatically turning on when the upper switch, implemented with a MOSFET or IGBT, is turned off. This operation occurs in continuous conduction mode (CCM), where the inductor current remains positive to keep the diode forward biased. If this condition is not met, the equations governing the converter's behavior will be altered.

In CCM, the switched topology operates in two distinct states, illustrated in Fig. 3. In the high state, when the control signal is high, the controllable switch S is turned on, connecting the input voltage to the LC circuit and allowing the inductor current to flow. This state, known as the on-time t_{on}, is maintained for a specific duration. Following that, the control signal transitions to the low state, causing the controllable switch to turn off, and the current is redirected through the diode. This state, known as the off-time t_{off}, is sustained for a specific duration.

The proposed buck converter is specifically designed to accept a 48-V input voltage and convert it to a 29-V output voltage. The converter functions at a switching frequency of 10 kHz. Under maximum load conditions, the minimum load resistance (R_{min}) is determined to be 3.9465 Ω. During CCM operation, the inductor is permitted to have a maximum ripple equivalent to 20 % of the average inductor current and the maximum load. Similarly, the capacitor is allowed to exhibit a maximum ripple of ±2 % of the average output voltage.

The steady-state duty cycle of the plant is represented as:

$$D = \frac{V_{out}}{V_{in}} \tag{2}$$

The upper limit of the average inductor current is indicated as:

$$I_{L,avg,max} = \frac{V_{out}}{R_{min}} \tag{3}$$

The maximum inductor ripple current, equal to 20 % of the average current, is indicated as:

$$\Delta I_L = 0.2 \times I_{L,avg,max} \tag{4}$$

The inductance value, denoted as L, of the inductor is given by:

$$L = \frac{V_{in}(1-D)D}{f_{sw}\Delta I_L} \tag{5}$$

The representation of the capacitor ripple voltage (ΔV_C) or output voltage ripple (ΔV_{out}) is expressed as follows, where it is equal to ±2 % of the average output voltage:

$$\Delta V_C = \Delta V_{out} = 0.04 \times V_{out} \tag{6}$$

The capacitance value, denoted as C, of the capacitor is expressed as:

$$C = \frac{V_{in}(1-D)D}{8Lf_{sw}{}^2\Delta V_C} \tag{7}$$

Table 2 presents the computed values for the parameters and components of the suggested buck converter.

2.3. Deriving transfer function of the proposed buck converter

In Section 2.1, a detailed and systematic analysis of the averaging-perturbation-linearization process of the SMPS is provided to derive the transfer function for the buck converter. The derivation considers the components of the converter such as input voltage (V_{in}), inductance (L), output capacitance (C_{out}), load resistance (R_{Load}), inductor current (i_L), capacitor current (i_C), inductor voltage

Table 3
Circuit analysis of the proposed buck converter in ON and OFF states.

	On-state (time interval: $0 < t < dT_s$)	Off-state (time interval: $dT_s < t < T_s$)	State-space averaging	
Derivation of state equations	$V_L = L\frac{di_L}{dt} = V_{in} - V_{out}\frac{di_L}{dt} = \frac{V_{in} - V_{out}}{L}$ $i_L = i_{out} + i_C$ $i_L = \frac{V_{out}}{R_{Load}} + C_{out}\frac{dV_C}{dt}$ $\frac{dV_C}{dt} = \frac{i_L}{C_{out}} - \frac{V_{out}}{R_{Load}C_{out}}$	$V_L = L\frac{di_L}{dt} = -V_{out}\frac{di_L}{dt} = \frac{-V_{out}}{L}$ $i_L = i_{out} + i_C$ $i_L = \frac{V_{out}}{R_{Load}} + C_{out}\frac{dV_C}{dt}$ $\frac{dV_C}{dt} = \frac{i_L}{C_{out}} - \frac{V_{out}}{R_{Load}C_{out}}$	**The averaged system matrix**	$A = \begin{bmatrix} 0 & \frac{-1}{L} \\ \frac{1}{C_{out}} & \frac{-1}{RC_{out}} \end{bmatrix}$
System matrices	$A_1 = \begin{bmatrix} 0 & \frac{-1}{L} \\ \frac{1}{C_{out}} & \frac{-1}{RC_{out}} \end{bmatrix}$	$A_2 = \begin{bmatrix} 0 & \frac{-1}{L} \\ \frac{1}{C_{out}} & \frac{-1}{RC_{out}} \end{bmatrix}$	**The averaged input matrix**	$B = \begin{bmatrix} \frac{D}{L} \\ 0 \end{bmatrix}$
Input matrices	$B_1 = \begin{bmatrix} \frac{1}{L} \\ 0 \end{bmatrix}$	$B_2 = \begin{bmatrix} 0 \\ 0 \end{bmatrix}$	**Averaged state-space equation** $\dot{x} = Ax + BV_{dc}$	$\begin{bmatrix} \frac{di_L}{dt} \\ \frac{dV_C}{dt} \end{bmatrix} = \begin{bmatrix} 0 & \frac{-1}{L} \\ \frac{1}{C_{out}} & \frac{-1}{RC_{out}} \end{bmatrix} \begin{bmatrix} i_L \\ V_C \end{bmatrix} + \begin{bmatrix} \frac{D}{L} \\ 0 \end{bmatrix} [V_{in}]$

(V_L), capacitor voltage (V_C), steady-state duty cycle (D), and small signal duty ratio (d). A step-by-step approach is followed to derive these equations.

The Laplace transform of the state and output equations, assuming a zero initial condition, is represented as:

$$sX(s) = AX(s) + BU(s) \tag{8}$$

$$Y(s) = CX(s) + DU(s)$$

The state equation is reformulated as follows:

$$sX(s) - AX(s) = BU(s) \tag{9}$$

$$(sI - A)X(s) = BU(s)$$

Multiplying both sides of Eq. (9) by $(sI - A)^{-1}$ results in:

$$X(s) = (sI - A)^{-1}BU(s) \tag{10}$$

Substituting Eq. (10) into the output equation of the plant yields:

$$Y(s) = \left[C(sI - A)^{-1}B + D\right]U(s) \tag{11}$$

The system's transfer function is expressed as:

$$G(s) = \frac{Y(s)}{U(s)} = C(sI - A)^{-1}B + D \tag{12}$$

Analyzing converters using AC small signals requires deriving the averaged state-space equation of the converters and introducing AC variations (perturbations) around the steady-state condition. To find the system's steady-state operating point, the time derivative in the state equation is set to zero, as shown in Eq. (1). The dynamic AC small signal model can be expressed as follows:

$$\widehat{x}(s) = (sI - A)^{-1}[(A_1 - A_2)X + (B_1 - B_2)V_{in}]\widehat{d}(s) \tag{13}$$

$$\frac{\widehat{x}(s)}{\widehat{d}(s)} = (sI - A)^{-1}[(A_1 - A_2)X + (B_1 - B_2)V_{in}]$$

The system's state variables, which consist of i_L and V_C, are selected based on the capacitor and inductor being the primary energy storage components of the buck converter. Therefore, the system vector x for the buck converter is defined as:

$$x = \begin{bmatrix} i_L \\ V_C \end{bmatrix} \tag{14}$$

Table 3 presents the analysis of the buck converter's operation in the CCM and the derivation of its averaged state-space equation.

By assuming that all parasitic resistances are negligible, the state variable vector X at the steady-state operation point, as derived from Eq. (1), can be reformulated as follows:

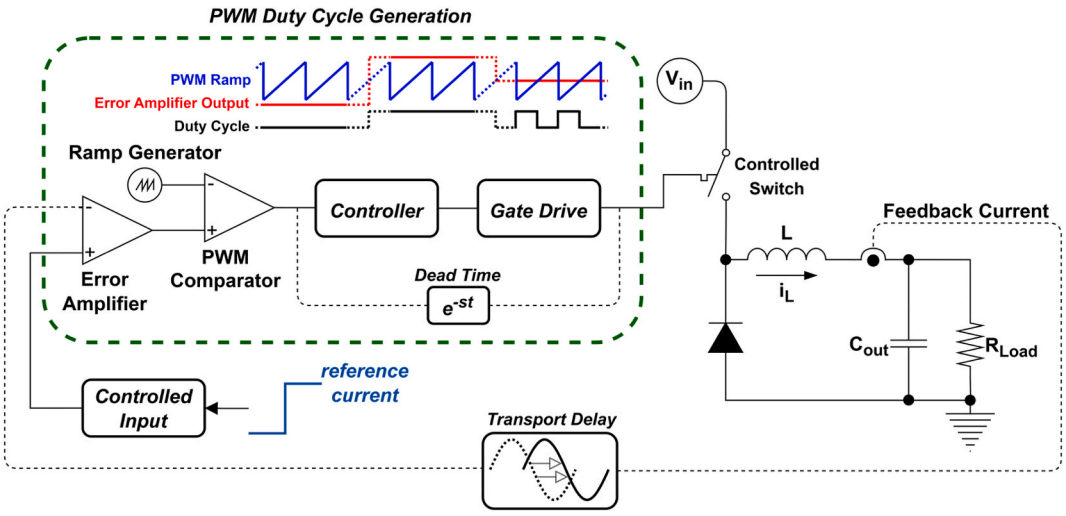

Fig. 4. The control feedback configuration of the asynchronous buck converter incorporating delays.

$$X = -A^{-1}BV_{in} = -\frac{adj\begin{bmatrix} 0 & \frac{-1}{L} \\ \frac{1}{C_{out}} & \frac{-1}{R_{Load}C_{out}} \end{bmatrix}}{det\begin{bmatrix} 0 & \frac{-1}{L} \\ \frac{1}{C_{out}} & \frac{-1}{R_{Load}C_{out}} \end{bmatrix}} \begin{bmatrix} \frac{D}{L} \\ 0 \end{bmatrix} V_{in} = \begin{bmatrix} \frac{{C_{out}}^2 DV_{in}}{R_{Load}} \\ DV_{in} \end{bmatrix} \tag{15}$$

By substituting Eq. (15) and the averaged system and input matrices obtained from Table 3 into Eq. (13), the following equation is obtained:

$$\frac{\widehat{x}(s)}{\widehat{d}(s)} = \frac{\begin{bmatrix} \widehat{i}_L \\ \widehat{V}_C \end{bmatrix}}{\widehat{d}(s)} = \begin{bmatrix} \frac{V_{in}(C_{out}R_{Load}s+1)}{C_{out}LR_{Load}s^2 + Ls + R_{Load}} \\ \frac{V_{in}R_{Load}}{C_{out}LR_{Load}s^2 + Ls + R_{Load}} \end{bmatrix} \tag{16}$$

By substituting the calculated values of the components for the desired buck converter into Eq. (16), the transfer function that relates the d to the i_L can be derived, yielding the following expression:

$$\frac{i_L(s)}{d(s)} = \frac{V_{in}}{L}\frac{s + \frac{1}{R_{Load}C_{out}}}{s^2 + \frac{s}{R_{Load}C_{out}} + \frac{1}{LC_{out}}} = (6.1455e4)\frac{s+1.6e4}{s^2 + 1600s + 8.0841e7} \tag{17}$$

3. Delays in digital control systems

Many encountered dynamic systems inherently possess a certain degree of time delay. When designing a controller for such systems, it becomes imperative to incorporate mechanisms that effectively address this delay. The duration of the delay may vary, ranging from insignificantly short intervals that can be disregarded to significantly longer durations that can severely impair system performance and even lead to instability.

Two primary categories of delay exist within dynamic systems:

- Distorting delays: These delays introduce distortions or alterations to the system's output signal, thereby impacting its overall behavior. Distorting delays can lead to phase shifts, amplitude variations, or other modifications that affect the system's response characteristics.
- Non-distorting delays: In contrast to distorting delays, non-distorting delays do not introduce any significant alterations or distortions to the system's output signal. Although these delays may cause a temporal shift in the system's response, they do not affect the fundamental properties or integrity of the output.

Understanding and categorizing delays into these two types is essential for analyzing and developing appropriate control strategies tailored to the specific characteristics of the delay in question. The unity feedback configuration of the asynchronous buck converter

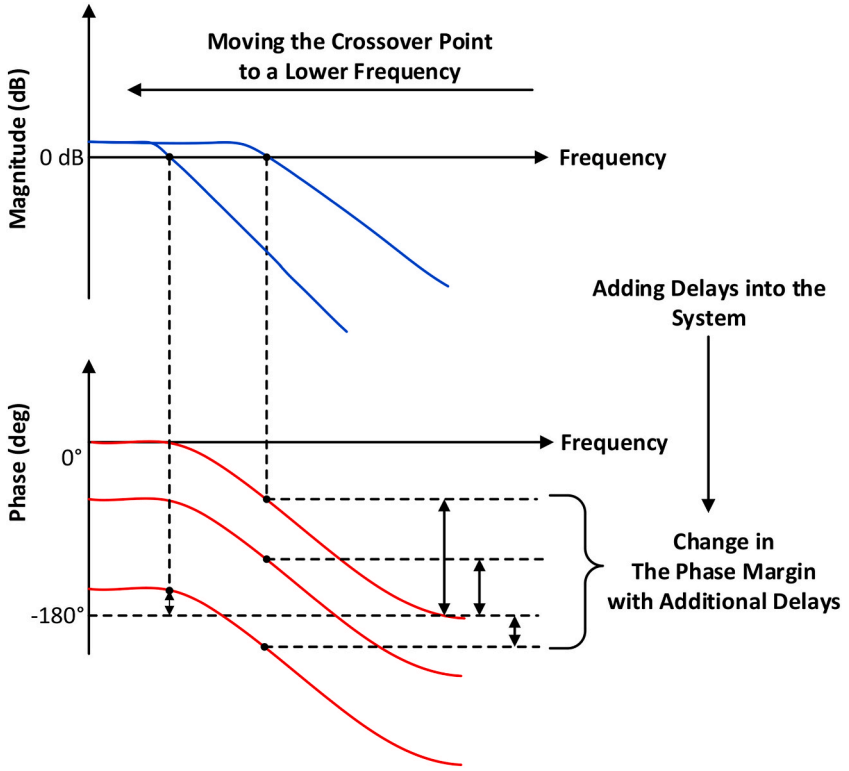

Fig. 5. The bode plot of an arbitrary second-order system in the presence of delays.

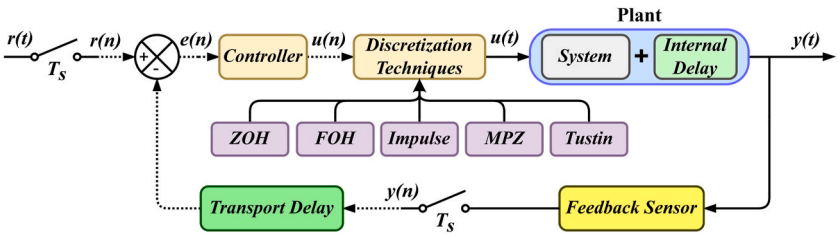

Fig. 6. Block structure of a digitally controlled nonlinear system with delays using various discretization techniques.

system with both distorting and non-distorting delays is given in Fig. 4.

The Bode plot of a generic second-order system provides valuable insights into its frequency response characteristics. In particular, the unity-gain frequency (crossover angular frequency) denotes the point at which the magnitude plot intersects the 0 dB line. This specific frequency allows you to assess the amount of phase margin present in the system when a feedback loop is established around it. By analyzing the phase response at the unity-gain frequency, it is possible to determine the phase margin, which signifies the extent of additional phase shift that the system can withstand before becoming unstable. The phase margin serves as an indicator of the system's stability robustness, demonstrating its capacity to handle disturbances or variations without entering an unstable state. Analyzing the Bode plot, especially at the crossover frequency, enables engineers to make informed decisions regarding the design and tuning of the feedback loop, ensuring that the system remains stable and meets the desired performance specifications. The Bode plot of an arbitrary second-order system is given in Fig. 5. The visual representation provided in the figure demonstrates that if additional delay is introduced into the system, either through transport delays or by delaying frequencies around the crossover frequency, it will affect the phase plot.

As a result, the phase margin will be diminished, potentially leading to an unstable closed-loop system. To mitigate this issue, one approach is to lower the bandwidth of the controller by shifting the crossover point to a lower frequency. By doing so, the phase margin can be restored. However, this adjustment comes at the cost of reducing the system's speed and responsiveness. The system's overall performance will be slower, resulting in decreased responsiveness to changes or disturbances. Thus, there is a trade-off between stability and system performance when addressing delay-related issues in the control design.

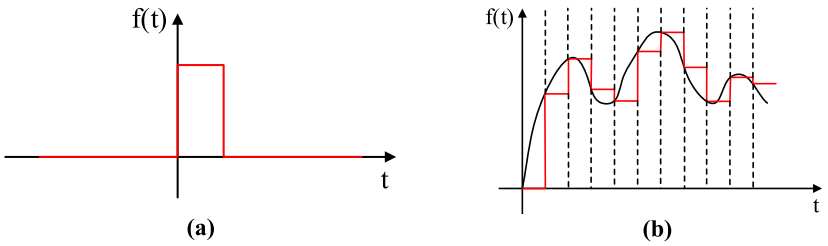

Fig. 7. The ZOH's time-domain analysis **(a)** The time-shifted and time-scaled $rect\left(\frac{t-T_s/2}{T_s}\right)$ function **(b)** Signal with piecewise constant $x_{ZOH}(t)$.

4. Implementation of various discretization techniques for the proposed buck converter

Discretization, in the realm of applied mathematics, refers to the process of converting continuous equations, models, variables, and functions into their discrete counterparts. This transformation is typically undertaken as a preliminary step to facilitate numerical evaluation and implementation on digital computers. In the domain of digital control systems, the controller is implemented on a computerized digital platform, operating based on measurements acquired at specific discrete time intervals before issuing commands to actuators. However, during the transition from a continuous system to a discrete system, some information is unavoidably lost, potentially impacting the performance of the control system. Moreover, the inclusion of discrete systems in the feedback loop introduces a delay that reduces the controller's bandwidth. Fig. 6 presents the unity feedback control structure for nonlinear systems with delays and various discretization techniques.

The selection of a suitable discretization approach becomes crucial due to the challenges posed by bandwidth, which represents the maximum frequency at which the control system can effectively respond. Various digitalization approaches or methods are commonly employed in control systems, including first-order hold (FOH), zero-order hold (ZOH), impulse response matching, and matched pole-zero (MPZ) technique, in dual-domain (both time and frequency) analysis). These techniques offer different trade-offs and characteristics, and choosing the right discretization method is of paramount importance to ensure the desired control system performance.

4.1. ZOH method

A zero-order hold, assuming one sample per time interval T_s, reconstructs the following continuous-time waveform from a sample sequence $x[n]$:

$$x_{ZOH}(t) = \sum_{n=-\infty}^{\infty} x[n].rect\left(\frac{t - T_s/2 - nT_s}{T_s}\right) \tag{18}$$

where $rect(.)$ is the rectangular function which is a special case of the more general boxer function given as:

$$rect\left(\frac{t - T_s/2}{T_s}\right) = H\left(t - \left(\frac{T_s}{2} - \frac{T_s}{2}\right)\right) - H\left(t - \left(\frac{T_s}{2} + \frac{T_s}{2}\right)\right) = H(t) - H(t - T_s) \tag{19}$$

where $H(x)$ is the Heaviside step function; the function centred at $\frac{T}{2}$ and has duration T, from 0 to T_s. The function $rect\left(\frac{t-T_s/2}{T_s}\right)$ and $x_{ZOH}(t)$ which is the piecewise-constant signal are depicted in Fig. 7(a) and (b), respectively.

The effective impulse response of Eq. (18) is derived as follows:

$$h_{ZOH}(t) = \frac{1}{T_s} rect\left(\frac{t}{T_s} - \frac{1}{2}\right) = f(x) = \begin{cases} \frac{1}{T_s}, if\ 0 \le t < T_s \\ 0, otherwise \end{cases} \tag{20}$$

The effective frequency response is determined by the continuous Fourier transform of the impulse response, which can be expressed as follows:

$$H_{ZOH}(f) = \mathscr{F}\{h_{ZOH}(t)\} = \frac{1 - e^{-i2\pi fT_s}}{i2\pi fT_s} = e^{-i\pi fT_s} sinc(fT_s) \tag{21}$$

where, in digital signal processing, $sinc(x)$ is the normalized $sinc$ function ($\frac{\sin(\pi x)}{\pi x}$) that is commonly employed. Transfer function of the ZOH is derived by implementing Laplace transform and substituting $s = i2\pi f$ as:

$$H_{ZOH}(s) = \mathscr{L}\{h_{ZOH}(t)\} = \frac{1 - e^{-sT_s}}{sT_s} \tag{22}$$

The conversion of the continuous-time transfer function of the buck converter and the designed controller into discrete form using the ZOH method, with a sampling frequency that is ten times higher than the switching frequency ($T_s = 1/10f_{sw}$), is represented as

follows:

$$G_{Buck(ZOH)}(z) = \frac{0.3071z^2 + 0.0454z - 0.2617}{z^2 - 1.845z + 0.8521} \tag{23}$$

4.2. FOH method

As a tracking model from a measured (or sampled) value of the plant output signal, this type of signal holder employs the unit ramp function for the entire interval between two consecutive sampling points. The piecewise linear signal equation of the FOH is defined by:

$$x_{FOH}(t) = \sum_{n=-\infty}^{\infty} x(nT_s) tri\left(\frac{1 - nT_s}{T_s}\right) \tag{24}$$

The solution of Eq. (24) results in effective impulse response given by:

$$h_{FOH}(t) = \frac{1}{T_s} tri\left(\frac{t}{T_s}\right) = f(x) = \begin{cases} \frac{1}{T_s}\left(1 - \frac{|t|}{T_s}\right), if\,|t| < T_s \\ 0, otherwise \end{cases} \tag{25}$$

where $tri(x)$ is the triangular function, whose graph take the shape of a triangle unlike a $rect(.)$ function of x used in the ZOH. The effective frequency response, which is obtained through the continuous Fourier transform of the impulse response in Eq. (25), can be represented as follows:

$$H_{FOH}(f) = \mathcal{F}\{h_{FOH}(t)\} = \left(\frac{e^{i\pi fT_s} - e^{-i\pi fT_s}}{i2\pi fT_s}\right)^2 = sinc^2(fT_s) \tag{26}$$

Transfer function of the FOH is derived by implementing Laplace transform and substituting $s = i2\pi f$ as:

$$H_{FOH}(s) = \mathcal{L}\{h_{FOH}(t)\} = \left(\frac{1 - e^{-sT_s}}{sT_s}\right)^2 \tag{27}$$

Discretization of the continuous-time transfer function of the buck converter and the designed controller by using the FOH method with a sampling frequency that is ten times greater than the switching frequency ($T_s = 1/10f_{sw}$), is expressed as follows:

$$G_{Buck(FOH)}(z) = \frac{0.6137z - 0.5229}{z^2 - 1.845z + 0.8521} \tag{28}$$

4.3. Impulse-response matching method

The impulse response of the continuous-time system, $h_c(t)$, is discretized through sampling to obtain the impulse response of the discrete-time system, $h[n]$, with a sampling period of T_s, as expressed by the following equation:

$$h[n] = T_s h_c(nT_s) \tag{29}$$

The analogue and digital frequencies of the system are related by $\omega = \Omega T_s$ or $e^{j\omega} = e^{j\Omega T_s}$ or $z = e^{sT_s}$ with the following equation:

$$H\left(e^{j\omega}\right) = \frac{1}{T_s} \sum_{k=-\infty}^{\infty} H_c\left(j\frac{\omega}{T_s} + j\frac{2\pi}{T_s}k\right) \tag{30}$$

where Ω is the continuous-time angular frequency in the unit of rad/s and ω is the discrete-time normalized angular frequency represented in radians per sample frequency in Hz. Since $z = e^{j\omega}$ on the unit circle and $s = j\Omega$ on the imaginary axis, transformation from s-plane to z-plane is given by:

$$H_{Impulse}(z) = \frac{1}{T_s} \sum_{k=-\infty}^{\infty} H_c\left(s - j\frac{2\pi}{T_s}k\right) \tag{31}$$

The transfer function of the continuous-time buck converter and the designed controller are converted into the discrete-time domain using the impulse-response matching method. This discretization process is carried out with a sampling frequency that is ten times higher than the switching frequency ($T_s = 1/10f_{sw}$). The resulting discrete representation is expressed as follows:

$$G_{Buck(Impulse)}(z) = \frac{0.6145z^2 - 0.5214z}{z^2 - 1.845z + 0.8521} \tag{32}$$

4.4. Tustin method

The Tustin method, also known as the bilinear approximation or trapezoidal integration method, offers a precise mapping from the s-plane to the z-plane. It utilizes a first-order Padé approximation of the natural logarithm function. When a discrete-time signal undergoes the Laplace transform, where each element of the discrete-time sequence is associated with a correspondingly delayed unit impulse, the outcome is the Z transform of the discrete-time sequence itself. By substituting $z = e^{sT_s}$, this method shifts each pole and zero location across the z-domain and constructs the corresponding transfer function.

Implementing this equality for the entire system is not unapplicable as it will result in a non-linear function. Hence, the linearization of t e^{sT_s} is required by using Taylor's series expansion of e^x as given by:

$$e^x = \sum_{n=0}^{\infty} \frac{x^n}{n!} \tag{33}$$

The implementation of Eq. (33) for the equality $z = e^{sT_s}$ is given by:

$$z = e^{sT_s} = 1 + sT_s + \frac{(sT_s)^2}{2} + \frac{(sT_s)^3}{6} + \frac{(sT_s)^4}{24} + \dots \tag{34}$$

Discarding the higher-order terms in Eq. (34) results in the first order approximation for z given by:

$$z \approx 1 + sT_s \tag{35}$$

Eq. (35) is a linear first order approximation of e^{sT_s}, but it can be improved by the implementation of a polynomial fraction in the form of:

$$z = \frac{a + bs}{c + ds} \tag{36}$$

This polynomial fraction expansion gives better and closer results to e^{sT_s} than the single polynomial given in Eq. (34). The polynomial fraction expansion is implemented by splitting e^{sT_s} into two exponentials given by:

$$z = e^{sT_s} = \left(e^{\frac{sT_s}{2}}\right)\left(e^{\frac{sT_s}{2}}\right) = \frac{e^{\frac{sT_s}{2}}}{e^{\frac{-sT_s}{2}}} = \frac{1 + \frac{sT_s}{2} + \frac{(sT_s)^2}{8} + \dots}{1 - \frac{sT_s}{2} + \frac{(sT_s)^2}{8} + \dots} \tag{37}$$

Discarding the higher-order terms in Eq. (37) results in more accurate first order approximation to e^{sT_s} given by:

$$z \approx \frac{1 + \frac{sT_s}{2}}{1 - \frac{sT_s}{2}} \tag{38}$$

One way to interpret the bilinear transform equation is that they are the linear first order approximation of e^{sT_s} and the discretization is carried out by replacing z with this approximation. To give an insight, the bilinear method can be explained by using trapezoidal integration method which is the integration of a given function as:

$$y(x) = \int_{x_0}^{x_1} f(x)dx \approx (x_1 - x_0)\left[\frac{f(x_0) + f(x_1)}{2}\right] \tag{39}$$

Adding another point x_2 and extending the $f(x)$ out, a second trapezoid between x_1 and x_2 is obtained. The approximated area for the whole section is given by:

$$y(x) = \int_{x_0}^{x_2} f(x)dx = \int_{x_0}^{x_1} f(x)dx + \int_{x_1}^{x_2} f(x)dx \tag{40}$$

$$y(x) \approx (x_1 - x_0)\left[\frac{f(x_0) + f(x_1)}{2}\right] + (x_2 - x_1)\left[\frac{f(x_1) + f(x_2)}{2}\right] \tag{41}$$

The generalized representation of the trapezoidal integration method to any point x_k is given by:

$$y_k = \Delta x\left[\frac{x_{k-1} + x_k}{2}\right] + y_{k-1} \tag{42}$$

Application of the trapezoidal integration for a system whose transfer function is $1/s$ performed by breaking it up by sample periods T_s represented by:

$$y(kT_s) = \int_0^{kT_s} x(t)dt = \int_{kT_s - T_s}^{kT_s} x(t)dt + \int_0^{kT_s - T_s} x(t)dt \tag{43}$$

$$y(kT_s) \approx T_s\left[\frac{x(kT_s) + x(kT_s - T_s)}{2}\right] + y(kT_s - T_s) \tag{44}$$

Arranging Eq. (44) and taking the z transform results in the following equation:

$$Y(z)\left(1-z^{-1}\right)=\frac{T_s}{2}X(z)\left(1+z^{-1}\right) \tag{45}$$

Rearranging Eq. (45) is required to get the transfer function of $Y(z)/X(z)$ as:

$$\frac{Y(z)}{X(z)}=\frac{T_s}{2}\frac{(1+z^{-1})}{(1-z^{-1})}=\frac{T_s}{2}\frac{(z+1)}{(z-1)} \tag{46}$$

Considering the starting s-domain transfer function $1/s$, the resulting transformation including the connection between continuous and discrete time domains is represented by:

$$\frac{Y(s)}{X(s)}=\frac{1}{s}\approx\frac{T_s}{2}\frac{(z+1)}{(z-1)} \tag{47}$$

Solving Eq. (47) for s approximately yields:

$$\mathrm{s}\approx\frac{2}{\mathrm{T_s}}\left(\frac{\mathrm{z}-1}{\mathrm{z}+1}\right) \tag{48}$$

The equation for approximating the transfer function in the z-domain from its continuous form in the s-domain, considering a sampling time of $\boldsymbol{T}_s$, can be represented as follows:

$$\mathrm{z}=\mathrm{e}^{\mathrm{sT_s}}\approx\frac{1+\frac{\mathrm{sT_s}}{2}}{1-\frac{\mathrm{sT_s}}{2}} \tag{49}$$

The transfer function of the continuous-time buck converter and the designed controller is converted into discrete-time using Tustin's method. This conversion is performed with a sampling frequency that is ten times higher than the switching frequency ($T_s = 1/10f_{sw}$). The resulting equation for the discrete-time representation is as follows:

$$G_{Buck(Tustin)}(z)=\frac{0.3067z^2+0.0454z-0.2613}{z^2-1.845z+0.8521} \tag{50}$$

4.5. MPZ method

The method known as the matched Z-transform, also referred to as pole-zero mapping or pole-zero matching, is a discretization technique that involves mapping the poles and zeros of the continuous-time system from the s-plane to the z-plane by substituting $z = e^{sT_s}$. This technique is commonly employed to transform a filter design in continuous time into a design for a digital filter with a sample interval of $T_s = \frac{1}{f_{sw}}$.

A typical zero-pole-gain representation of an analogue filter transfer function is given by:

$$H(s)=k_a\frac{(s-z_1)(s-z_2)\ldots s-z_M}{(s-p_1)(s-p_2)\ldots s-p_N}=k_a\frac{\prod_{i=1}^{M}(s-z_i)}{\prod_{i=1}^{N}(s-p_i)} \tag{51}$$

Transformation from continuous-time (s-plane) to discrete-time (z-plane) is given by:

$$H(z)=k_d\frac{(1-e^{z_1T_s}z^{-1})(1-e^{z_2T_s}z^{-1})\ldots(1-e^{z_MT_s}z^{-1})}{(1-e^{p_1T_s}z^{-1})(1-e^{p_2T_s}z^{-1})\ldots(1-e^{p_NT_s}z^{-1})}\ H(z)=k_d\frac{\prod_{i=1}^{M}(1-e^{z_iT_s}z^{-1})}{\prod_{i=1}^{N}(1-e^{p_iT_s}z^{-1})} \tag{52}$$

To normalize the desired gain, the gain k_d must be set to match the gain of the analogue filter k_a at DC by setting $s = 0$ and $z = 1$ and solving for k_d.

The complete four step process of the MPZ can summarized as:

- z-plane mapping from each pole and zero
- If necessary, adding zeros at infinity
- If necessary, removing zeros at infinity to make a strictly proper function
- Adjusting the gain

In this method, it has been suggested that the digital system could be made more efficient by artificially adding zeros at z = -1, but this improvised solution is only a temporary solution. Hence, the MPZ is avoided in preference for impulse response matching or bilinear transformation. Although this method can be used to develop perfectly functional filters, it is not commonly employed because

Table 4
An in-depth comparison of the discretization techniques mentioned in the study.

Discretization Technique	Description	Advantages	Limitations	Applicability
ZOH	Holds constant values over discrete intervals	Simple implementation	Introduces initial delay	General
FOH	Approximates using first-order system	Captures initial slope, smoother transitions	Limited accuracy for rapidly changing signals	General
Impulse response matching	Matches discrete impulse response to continuous	Accurate representation of dynamics	Sensitive to noise, complex implementation	Critical control accuracy
Tustin	Maps using bilinear transformation	Accurate representation of dynamics	Frequency warping, phase shifts	General, stable systems
MPZ	Matches poles and zeros between domains	Retains pole and zero locations, accurate	Complex poles can lead to instability	Accurate representation

Table 5
A concise comparison of the discussed discretization techniques considering the impacts of disturbance and time delays.

Discretization Technique	Disturbance Handling	Impact of Time Delay	Additional Notes
ZOH	Struggles with effective handling due to discrete-time nature. Can result in oscillations and inaccuracies.	Inherent delay can introduce phase shifts and impact stability. High-frequency components might be distorted.	Limited suitability for handling disturbances and managing time delay.
FOH	Relatively better disturbance rejection due to consideration of initial derivatives. Large disturbances can still cause overshoot and oscillations.	Delay can introduce phase shifts. Integration of slope information mitigates high-frequency distortion to some extent.	Improved disturbance handling compared to ZOH.
Impulse response matching	Challenges in handling disturbances. Aligning impulse responses may not lead to optimal disturbance rejection.	Significant phase shifts can impact stability, especially at higher frequencies.	Less suitable for disturbance rejection and time delay management compared to other methods.
Tustin	Performs reasonably well in handling disturbances due to bilinear mapping.	Mapping introduces phase shifts, affecting frequency response. Balance between frequency response and delay management.	Balanced approach for handling disturbances and managing time delay.
MPZ	Tends to improve disturbance rejection by preserving continuous-time dynamic behavior.	Provides better control over time delay effects by matching poles and zeros. Demands more computational resources.	Suitable for systems requiring enhanced disturbance rejection and delay management.

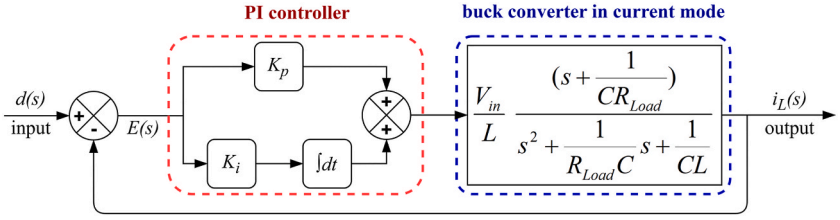

Fig. 8. The unity feedback configuration of a PI controlled buck converter.

it does not preserve any unique time or frequency-domain characteristics.

The continuous-time transfer function of the buck converter and the designed controller is discretized using the MPZ method. This discretization is performed with a sampling frequency that is ten times higher than the switching frequency ($T_s = 1/10f_{sw}$). The resulting equation for the discrete-time representation is as follows:

$$G_{Buck(MPZ)}(z) = \frac{0.6141z - 0.5233}{z^2 - 1.845z + 0.8521} \tag{53}$$

A comparison table summarizing the discussed discretization techniques is given in Table 4.

Table 5 provides a concise comparison of how each discretization technique handles disturbances and time delays, along with additional notes to highlight their relative strengths and weaknesses in these aspects. It is important to note that the suitability of each technique can vary based on the specific control system requirements and the nature of the disturbances and time delays present.

Table 6
The proposed buck converter design and control criteria.

Parameters	Value
Crossover (cutoff frequency)	between the range of 1/10th to 1/8th of switching frequency
Phase margin	greater than 45°
Gain margin	greater than 10 dB
The slope of the gain curve at the crossover frequency	≈-20 db/decade
Steady-state error	<2% for step input

Table 7
Step response characteristics of the proposed buck converter.

Step response characteristics	Open-loop buck converter	Closed-loop PI controlled buck converter
Rise time (s)	2.7203e-4	1.9402e-4
Settling time (s)	4.1803e-4	9.1124e-4
Settling minimum	10.9681	0.9006
Settling maximum	12.2004	0.9902
Overshoot (%)	0.31	0
Undershoot (%)	0	0
Peak	12.2004	0.9902
Peak time (s)	6.50483–4	0.0021

Table 8
Frequency response characteristics of the proposed buck converter.

Stability margin from frequency response data	Open-loop buck converter	Closed-loop PI controlled buck converter
Gain margin (dB)	Infinite	Infinite
Gain margin	–	–
Crossover frequency (rad/s)		
Phase margin (deg.)	90.2803	−180
Phase margin	6.2664e+4	0
Crossover frequency (rad/s)		
Delay margin (s)	2.5147e-5	Infinite
Delay margin	6.2664e+4	0
Crossover frequency (rad/s)		

5. PI controller design and control performance analysis

The plant's mathematical model is derived using state-space averaging and AC small signal techniques, allowing for the prediction of its response and observation of its behavior in both the time and frequency domains. Control systems are designed and implemented to improve important dynamic properties of the plant, including stability, response time, steady-state error, and oscillations present in both the transient and steady-state phases. Among the various controller structures available, the proportional-integral (PI) feedback compensator is commonly employed due to its simplicity in design, ease of understanding, and high level of effectiveness. Fig. 8 depicts the unity feedback structure of the proposed buck converter.

The design specifications for the PI controller are provided in Table 6, outlining the necessary criteria for its proper configuration based on SMPSs stable operation.

The proportional gain (K_p) is set to 0.21, while the integral gain (K_i) is determined as 709. When considering the negative unity feedback system comprising the designed PI controller and the transfer functions of the buck converter on the forward path, the resulting closed-loop transfer function can be expressed as follows:

$$\frac{i_L(s)}{d(s)} = \frac{G_{PI}(s)G_{Buck}(s)}{1 + G_{PI}(s)G_{Buck}(s)} \tag{54}$$

when the phase crosses −180°, the system goes into positive feedback and the plus sign int the denominator of the feedback transfer function changes to minus. Accordingly, the positive feedback of the system is given by:

$$\frac{i_L(s)}{d(s)} = \frac{G_{PI}(s)G_{Buck}(s)}{1 - G_{PI}(s)G_{Buck}(s)} \tag{55}$$

The DC (static) gain of the system which is the ratio of the steady state output to its constant input (unit step response) can be calculated by using final value theorem as:

$$\mathscr{L}\left(y_{step}(t)\right) = G_{PI}(s)G_{Buck}(s)\frac{1}{s} \tag{56}$$

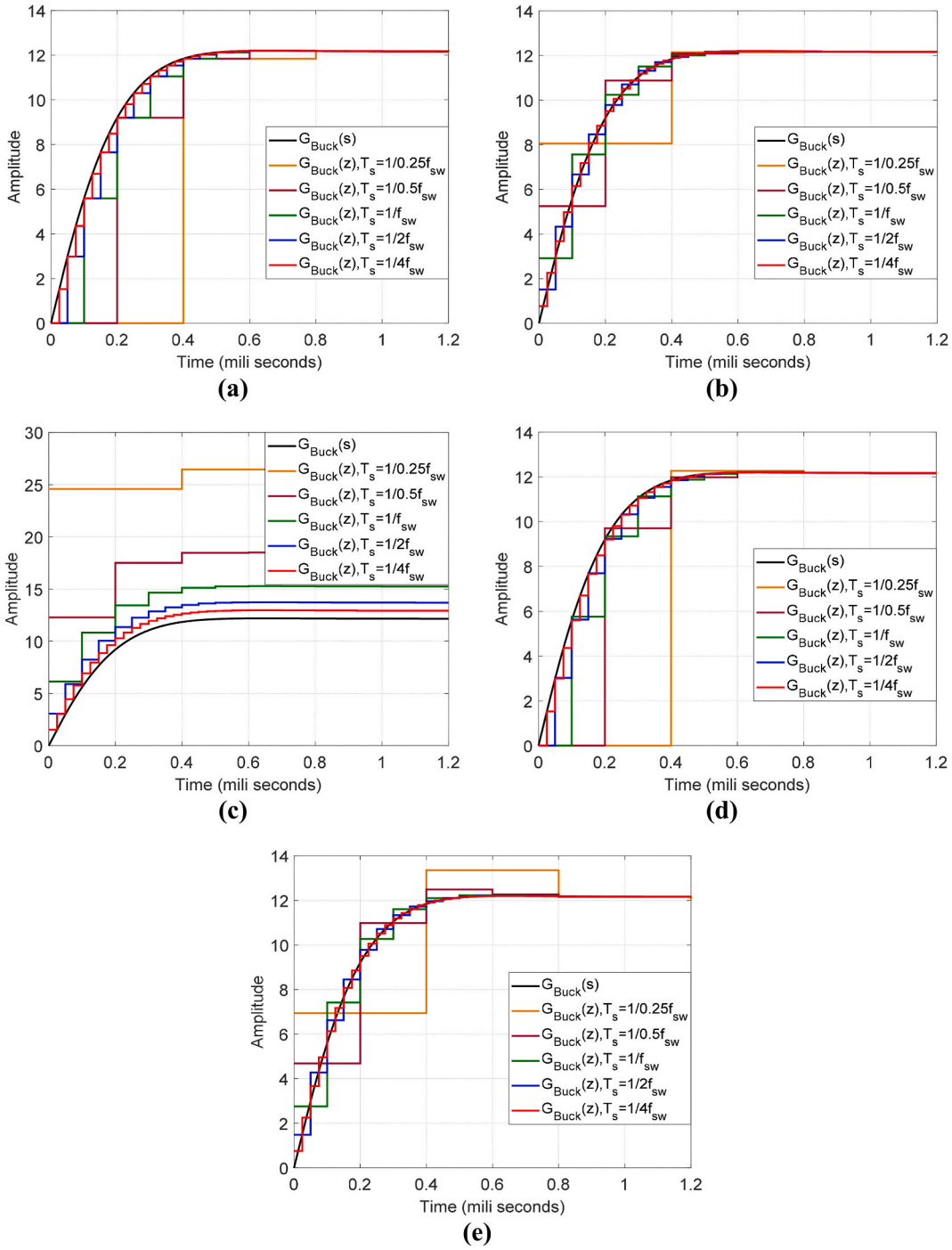

Fig. 9. Step responses for various sample times based on the switching frequency of the proposed buck converter **a)** $G_{Buck(ZOH)}(z)$, **b)** $G_{Buck(FOH)}(z)$, **c)** $G_{Buck(Impulse)}(z)$, **d)** $G_{Buck(MPZ)}(z)$, and **e)** $G_{Buck(Tustin)}(z)$ for varying sample times.

Table 9
Step response characteristics of the proposed buck converter discretized by using different methods and varying sample times.

Step response characteristics	Discretization methods with varying sample times based on switching frequency									
	ZOH method		FOH method		Impulse invariant method		Tustin method		MZP method	
	$\frac{1}{2f_{sw}}$	$\frac{1}{10f_{sw}}$	$\frac{1}{2f_{sw}}$	$\frac{1}{10f_{sw}}$	$\frac{1}{2f_{sw}}$	$\frac{1}{10f_{sw}}$	$\frac{1}{2f_{sw}}$	$\frac{1}{10f_{sw}}$	$\frac{1}{2f_{sw}}$	$\frac{1}{10f_{sw}}$
Rise time (s)	2.5e-4	2.8e-4	2.5e-4	2.7e-4	2.5e-4	2.7e-4	2.5e-4	2.7e-4	2.5e-4	2.8e-4
Settling time (s)	4.5e-4	4.2e-4	4.5e-4	4.2e-4	4.5e-4	4.2e-4	4e-4	4.2e-4	4.5e-4	4.2e-4
Settling minimum	11.0479	11.0479	11.3108	10.9857	12.8660	11.2938	11.3341	10.9865	11.0693	11.0488
Settling maximum	12.2004	12.2004	12.1993	12.2003	13.7368	12.5076	12.2063	12.2006	12.2010	12.2004
Overshoot (%)	0.31	0.31	0.3014	0.3096	0.2706	0.3021	0.3586	0.3116	0.3151	0.3102
Undershoot (%)	0	0	0	0	0	0	0	0	0	0
Peak	12.2004	12.2004	12.1993	12.2003	13.7368	12.5076	12.2063	12.2006	12.2010	12.2004
Peak time (s)	6.5e-4	6.5e-4	6.5e-4	6.5e-4	6.5e-4	6.5e-4	6e-4	6.4e-4	6.5e-4	6.5e-4

$$DC\ gain = \lim_{t\to\infty} y_{step}(t) = \lim_{s\to 0} s\left[G_{PI}(s)G_{Buck}(s)\frac{1}{s}\right] = \lim_{s\to 0} G_{PI}(s)G_{Buck}(s) \tag{57}$$

$$Dc\ gain = \lim_{s\to 0}\left(\frac{0.21s+709}{s}\right)\left(\frac{7.602\times 10^{-4}s+12.16}{1.237\times 10^{-8}s^2+1.979\times 10^{-4}s+1}\right) = infinite \tag{58}$$

It is important to note that for extremely large and small gains, the behavior of the system transfer function is nearly the same for both positive and negative feedback structures. Thus, even if the obtained phase margin from the frequency response data for the closed-loop system is -180°, it remains stable. Instability occurs when $|G_{PI}(s)G_{Buck}(s)| \approx 1$ and negative phase margin is present. Therefore, what truly matters is ensuring that the loop is not in positive feedback, particularly at or near the gain crossover frequency, rather than focusing on the calculated combination of gain margin and phase margin.

The step response characteristics of the proposed system are provided in Table 7 for both the open-loop and closed-loop configurations with the PI controller.

Table 8 presents the stability margins of the proposed system, which were obtained from the frequency response data, for both the open-loop and closed-loop configurations.

6. Results and discussions

There is no definitive best discretization method for the transfer function of a buck converter, as the choice depends on various factors such as the specific requirements of the system, desired performance, computational resources, and implementation constraints. Different discretization methods have different characteristics and may be suitable for different scenarios. Fig. 9 illustrates the step responses corresponding to different sample times obtained through the utilization of various discretization methods, which are based on the switching frequency of the proposed buck converter. The findings presented in Fig. 9, along with the derived numeric results in Table 9, unequivocally demonstrate that Tustin's method outperforms the other investigated discretization methods when applied to the step response analysis of the proposed buck converter in continuous time. The superior performance of Tustin's method is evident through its ability to yield the most favorable outcomes in terms of response characteristics.

Based on the frequency response illustrated in Fig. 10 and the corresponding numeric results presented in Table 10, it is evident that Tustin's method outperforms the other examined discretization techniques in terms of accurately capturing the frequency response characteristics of the proposed buck converter in continuous time. The superior performance of Tustin's method is substantiated by its ability to yield the most favorable outcomes and accurately reproduce the frequency response characteristics across the desired frequency range.

Table 10 reveals a noteworthy observation indicating that the utilization of specific discretization techniques with significant sample times can lead to instability in the transfer function of the proposed buck converter. Tables 9 and 10 further confirm that selecting a small sample time for system discretization does not universally guarantee the best outcomes. These tables likely demonstrate instances where employing a small sample time resulted in suboptimal or unfavorable results in terms of system performance or stability. This highlights the importance of carefully considering the specific requirements, dynamics, and constraints of the system when determining an appropriate sample time for discretization. The choice of sample time should be a well-informed decision, considering factors such as computational resources, desired accuracy, stability requirements, and implementation constraints to achieve the desired performance trade-offs.

The performance of the aforementioned discretization methods in terms of transient response compared to continuous time, considering the inherited process delay of 0.01 ms and the transport delay of 0.05 ms, is demonstrated in Figs. 11 and 12.

It is clear that the Tustin discretization technique stands out as an effective method for controller design in scenarios involving highly non-linear behaviors of systems like the DC-DC buck converter. This technique offers a balance between accurately capturing system dynamics, addressing non-linearities, and maintaining stability—a crucial requirement for control applications. In the context of a DC-DC buck converter exhibiting pronounced non-linear behaviors, the Tustin discretization technique offers distinct advantages

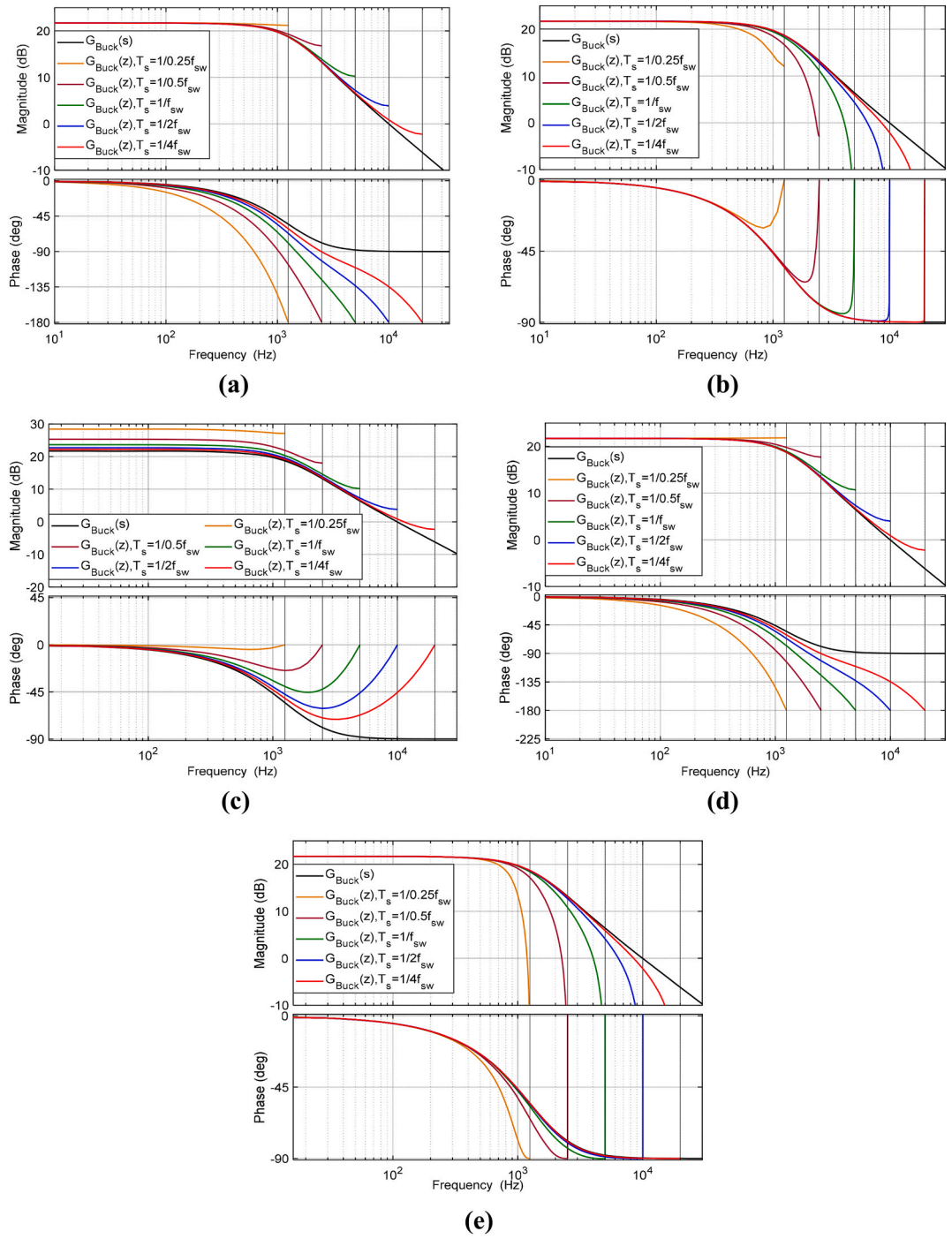

Fig. 10. Bode plots for various sample times based on the switching frequency of the proposed buck converter **a)** $G_{Buck(ZOH)}(z)$, **b)** $G_{Buck(FOH)}(z)$, **c)** $G_{Buck(Impulse)}(z)$, **d)** $G_{Buck(MPZ)}(z)$, and **e)** $G_{Buck(Tustin)}(z)$ for varying sample time.

over other methods due to its inherent ability to handle both continuous-time and discrete-time domain characteristics simultaneously. This is particularly pertinent in scenarios where non-linearities arise due to rapid changes in the input voltage, load variations, and inherent switching dynamics of the converter. Considering these attributes, the Tustin discretization technique emerges as a compelling choice for controller design in the context of a DC-DC buck converter with highly non-linear behaviors. Its capacity to faithfully capture system dynamics, maintain stability, and effectively address frequency response nuances while accommodating non-linearities positions it as a robust solution for control system design, enabling optimal performance in the presence of intricate system behaviors.

Table 10
Frequency response characteristics of the proposed buck converter discretized by using different methods and varying sample times.

	Discretization methods with varying sample times based on switching frequency									
	ZOH method		FOH method		Impulse invariant method		Tustin method		MZP method	
Frequency response stability margin	$\frac{1}{2f_{sw}}$	$\frac{1}{10f_{sw}}$	$\frac{1}{2f_{sw}}$	$\frac{1}{10f_{sw}}$	$\frac{1}{2f_{sw}}$	$\frac{1}{10f_{sw}}$	$\frac{1}{2f_{sw}}$	$\frac{1}{10f_{sw}}$	$\frac{1}{2f_{sw}}$	$\frac{1}{10f_{sw}}$
Gain margin (dB)	0.6406	3.2523	Inf	Inf	Inf	Inf	Inf	Inf	0.63	3.25
Gain margin Crossover frequency (rad/s)	6.29e4	3.14e5	–	–	–	–	–	–	6.28e-4	3.14e5
Phase margin (deg.)	Inf	72.03	91.12	90.31	Inf	108.18	90.29	90.29	Inf	72.03
Phase margin Crossover frequency (rad/s)	–	6.37e4	4.06e4	6.08e4	–	6.37e4	4.01e4	6.07e4	–	6.37e4
Delay margin (s)	–	1.97	0.78	2.59	0	3	0.79	2.59	–	1.97
Delay margin Crossover frequency (rad/s)	–	6.37e4	4.06e4	6.08e4	–	6.37e4	4.01e4	6.07e4	–	6.37e4
Closed-loop stable	No	Yes	Yes	Yes	Yes	Yes	Yes	Yes	No	Yes

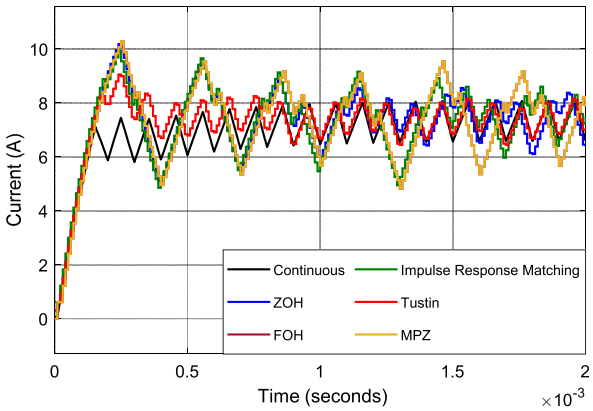

Fig. 11. Transient response of current control buck converter with the implementation of discussed discretization methods.

7. Conclusion and future work

This research encompassed a comprehensive investigation aimed at enhancing the understanding of the dynamic behavior, control algorithms optimization, system efficiency improvement, and reliable power conversion in PV applications through the analysis of a DC-DC buck converter. The objective was to delve into various aspects of PV system performance and uncover key strategies for enhancing the operation and control of buck converters.

Key areas of focus included discretization techniques, effective sample time selection considering system delays, and both time and frequency domain analysis. By thoroughly examining these aspects, the researchers aimed to shed light on the best practices for achieving accurate and efficient power conversion in PV applications. To address the non-linear behavior inherent in buck converters and improve digital control, several approaches were explored. Accurate modeling and identification of non-linear elements, the development of advanced control algorithms accounting for non-linearities, implementation of adaptive control techniques, and utilization of feedback mechanisms to compensate for deviations from linearity were identified as effective strategies. These strategies aimed to mitigate the impact of non-linear behavior and enable digital control systems to achieve improved accuracy, stability, and transient response in regulating the buck converter's output waveforms.

The results of this study showcased the superiority of the trapezoidal integration method, commonly known as the bilinear approximation or Tustin's approach, over other commonly used discretization methods such as FOH, ZOH, impulse response matching, and MPZ techniques. The researchers observed that the bilinear approximation exhibited exceptional performance in dual-domain (time and frequency) analysis. Notably, it bridged the gap between the continuous-time and discrete systems by closely matching frequency domain characteristics. This finding underscores the significance of the bilinear approach in preserving the frequency characteristics of the original continuous-time system during discretization. The employment of this method ensured an accurate representation of the frequency domain in the discrete system, which is crucial for maintaining the desired performance of the buck converter.

Moving forward, future work can explore further enhancements in PV system performance through the investigation of alternative discretization techniques and improved sample time selection methods that account for system delays. By evaluating different discretization methods and refining sample time selection approaches, researchers can refine the control strategies for buck converters and optimize their operation under various operating conditions.

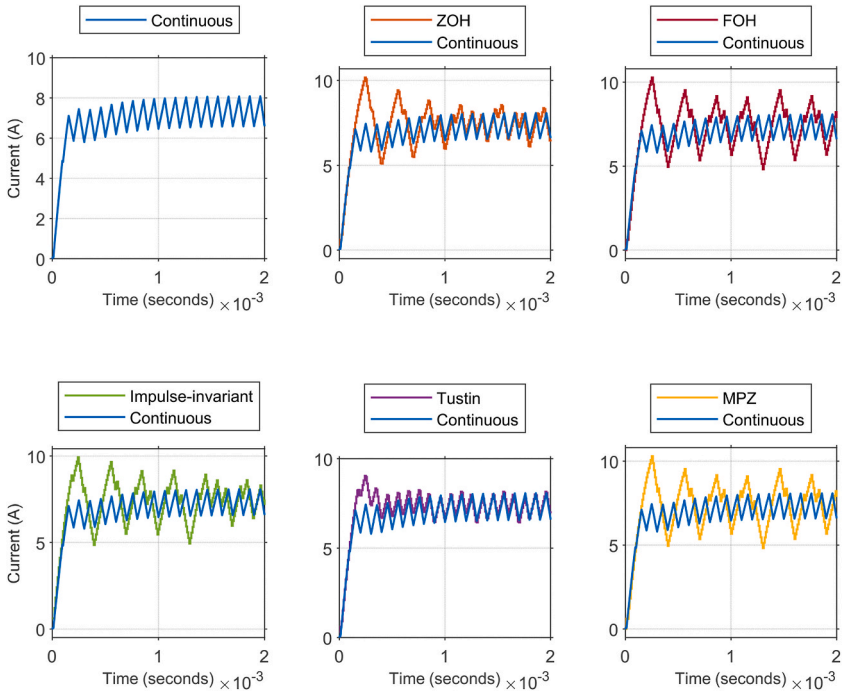

Fig. 12. The binary comparison of the discussed discretization methods for the proposed current control buck converter.

Author contribution statement

Cağfer Yanarateş: Aytaç Altan: Conceived and designed the experiments; Performed the experiments; Analyzed and interpreted the data; Contributed reagents, Materials, analysis tools or data; Wrote the paper. Serkan Okur: Conceived and designed the experiments; Performed the experiments; Analyzed and interpreted the data; Contributed reagents, materials, analysis tools or data.

Data availability statement

Data will be made available on request.

Declaration of competing interest

The authors declare that they have no known competing financial interests or personal relationships that could have appeared to influence the work reported in this paper.

References

[1] M.K.H. Rabaia, M.A. Abdelkareem, E.T. Sayed, K. Elsaid, K.J. Chae, T. Wilberforce, A.G. Olabi, Environmental impacts of solar energy systems: a review, Sci. Total Environ. 754 (2021), 141989.
[2] M. Mansoor, A.F. Mirza, Q. Ling, M.Y. Javed, Novel Grass Hopper optimization based MPPT of PV systems for complex partial shading conditions, Sol. Energy 198 (2020) 499–518.
[3] H.A. Khawaldeh, M. Al-Soeidat, M. Farhangi, D.D.C. Lu, L. Li, Efficiency improvement scheme for PV emulator based on a physical equivalent PV-cell model, IEEE Access 9 (2021) 83929–83939.
[4] I. Worighi, A. Maach, A. Hafid, O. Hegazy, J. Van Mierlo, Integrating renewable energy in smart grid system: architecture, virtualization and analysis, Sustainable Energy, Grids and Networks 18 (2019), 100226.
[5] A.N. Ali, K. Premkumar, M. Vishnupriya, B.V. Manikandan, T. Thamizhselvan, Design and development of realistic PV emulator adaptable to the maximum power point tracking algorithm and battery charging controller, Sol. Energy 220 (2021) 473–490.
[6] R. Ayop, C.W. Tan, Rapid prototyping of photovoltaic emulator using buck converter based on fast convergence resistance feedback method, IEEE Trans. Power Electron. 34 (9) (2018) 8715–8723.
[7] M. Chaker, A. El Houre, D. Yousfi, M. Kourchi, M. Ajaamoum, H. Idadoub, J. Bouchnaif, Development of a PV emulator using SMPS converter and a model selection mechanism for characteristic generation, Sol. Energy 239 (2022) 117–128.
[8] I.D. Jayawardana, C.N.M. Ho, M. Pokharel, G.E. Valderrama, A fast-dynamic control scheme for a power-electronics-based PV emulator, IEEE J. Photovoltaics 11 (2) (2020) 485–495.
[9] S. Mobayen, D. Baleanu, Stability analysis and controller design for the performance improvement of disturbed nonlinear systems using adaptive global sliding mode control approach, Nonlinear Dynam. 83 (2016) 1557–1565.
[10] S.S. Ge, F. Hong, T.H. Lee, Robust adaptive control of nonlinear systems with unknown time delays, Automatica 41 (7) (2005) 1181–1190.
[11] A.M. Dabroom, H.K. Khalil, Output feedback sampled-data control of nonlinear systems using high-gain observers, IEEE Trans. Automat. Control 46 (11) (2001) 1712–1725.

[12] D. Clemente-López, J.M. Munoz-Pacheco, J.D.J. Rangel-Magdaleno, A review of the digital implementation of continuous-time fractional-order chaotic systems using FPGAs and embedded hardware, Arch. Comput. Methods Eng. 30 (2) (2023) 951–983.
[13] B. Rong, X. Rui, L. Tao, G. Wang, Theoretical modeling and numerical solution methods for flexible multibody system dynamics, Nonlinear Dynam. 98 (2019) 1519–1553.
[14] T. Kërçi, M.A.A. Murad, I. Dassios, F. Milano, On the impact of discrete secondary controllers on power system dynamics, IEEE Trans. Power Syst. 36 (5) (2021) 4400–4409.
[15] H. Tan, H. Zhang, J. Peng, Z. Jiang, Y. Wu, Energy management of hybrid electric bus based on deep reinforcement learning in continuous state and action space, Energy Convers. Manag. 195 (2019) 548–560.
[16] A.M. Dabroom, H.K. Khalil, Output feedback sampled-data control of nonlinear systems using high-gain observers, IEEE Trans. Automat. Control 46 (11) (2001) 1712–1725.
[17] Y. Zhang, O. Kostyukova, K.T. Chong, A new time-discretization for delay multiple-input nonlinear systems using the Taylor method and first order hold, Discrete Appl. Math. 159 (9) (2011) 924–938.
[18] A. Seuret, F. Gouaisbaut, E. Fridman, Stability of discrete-time systems with time-varying delays via a novel summation inequality, IEEE Trans. Automat. Control 60 (10) (2015) 2740–2745.
[19] K. Yang, G.Q. Wu, X.D. Zhang, The control technology of BUCK converter, Appl. Mech. Mater. 150 (2012) 240–244.
[20] D. Rowell, State-space representation of LTI systems, URL: http://web.mit.edu/2.14/www/Handouts/StateSpace.pdf, 2002, 1-18.
[21] G. Herbst, A building-block approach to state-space modeling of DC-DC converter systems. J 2 (3) (2019) 247–267.
[22] P. Azer, A. Emadi, Generalized state space average model for multi-phase interleaved buck, boost and buck-boost DC-DC converters: transient, steady-state and switching dynamics, IEEE Access 8 (2020) 77735–77745.
[23] W.M. Polivka, P.R.K. Chetty, R.D. Middlebrook, State-space average modelling of converters with parasitics and storage-time modulation, in: 1980 IEEE Power Electronics Specialists Conference, IEEE, 1980, June, pp. 119–143.
[24] G. Suman, B.P. Kumar, M.S. Kumar, B.C. Babu, K.R. Subhashini, Modeling, analysis and design of synchronous buck converter using state space averaging technique for pv energy system, in: 2012 International Symposium on Electronic System Design (ISED), IEEE, 2012, December, pp. 281–285.